Preparation and Magnetic Properties of Fe/Si/C/N Ceramics Derived from a Polymeric Precursor

Junping Li,[1,2] Zhijie Zhang,[1] Zhimin Zheng,[1] Li Guo,[1,2] Guiyun Xu,[1] Zemin Xie[1]

[1]*Laboratory of Advanced Polymer Materials, Center for Molecular Science, Institute of Chemistry, Chinese Academy of Sciences, Beijing 100080, People's Republic of China*
[2]*Graduate University of Chinese Academy of Sciences, Beijing 100080, People's Republic of China*

Received 1 December 2006; accepted 3 January 2007
DOI 10.1002/app.26161
Published online 26 April 2007 in Wiley InterScience (www.interscience.wiley.com).

ABSTRACT: Iron-containing polysilazanes (PSZI) were prepared by the amine displacement reaction along with heat-induced vinyl crosslinking reactions between Fe[N(Si-$Me_2Vi)_2]_3$ (Vi = $-CH{=}CH_2$) and polysilazane containing $-Si-Vi$ (PVSZ). The PSZIs were converted into magnetic ceramics by the pyrolysis in N_2. The ceramics produced were investigated by X-ray diffraction, transmission electron microscope and vibrating sample magnetometer at room temperature. It was indicated that α-Fe is the only magnetic crystalline embedded in the amorphous Si/C/*N*-based matrix from 500 to 900°C. Moreover, the sample prepared at 500°C showed few hysteresis at room temperature, consistent with the behavior of superparamagnetic particles, which was confirmed by the zero-field-cooled and field-cooled magnetization measurement. Additionally, the results indicated that the magnetic properties of the ceramics could be tuned by controlling the content of iron and the pyrolysis temperature. This flexibility may be advantageous for some particular magnetic materials applications. © 2007 Wiley Periodicals, Inc. J Appl Polym Sci 105: 1786–1792, 2007

Key words: polysilazane; precursor; pyrolysis; magnetic ceramics; α-Fe

INTRODUCTION

Since the pioneering work of Yajima et al. discovered a promising approach to synthesize polymeric ceramics precursors for use in the fabrication of ceramic fibers, coatings, and binders,[1,2] intense research has been focused on the elaboration of SiC, Si_3N_4, or Si/C/*N*-based materials from organosilicon precursors, especially in the field of fibers or matrices via liquid and fusible precursors. Using this process, high purity products with a completely homogeneous distribution of the elements on an atomic scale and controllable microstructures can be obtained at relatively low temperatures. Furthermore, synthesis and crosslinking allow the control of the physical and chemical properties of the precursors, which provides processing opportunities for the preparation of ceramic monoliths, fibers, films, and powders. Another important advantage about this route is to prepare silicon-based multicomponent ceramics through chemical modification of silicon-based polymeric precursor. In this progress, desired elements (such as B, Ti, Zr, Hf, Ta, and Mg) for functional modified aids can be introduced to the precursors and the chemical composition including the desired elements can be regulated at the molecular or atomic level, which is expected to produce new types of high-performance silicon-based ceramic composites.[3–7]

On the other hand, iron has the highest magnetic moment from all 3d transition metals, which makes their stable nanoparticles or composites highly promising for applications in magnetic sensors,[8] microwave absorptive materials,[9] biomolecular separations,[10] and magnetic drug carriers.[11] Recently, some groups have focused on the research of the Si/C/Fe ceramics that were obtained from the polyferrocenylsilanes and their ramifications. The incorporation of iron into such ceramics is desirable as it will introduce interesting magnetic property.[12–16] But to the best of our knowledge, few investigations have focused on Fe/Si/C/N ceramics.

In 2003, our laboratory successfully synthesized the iron-containing polysilazanes (PSZI) as precursor of Si-C-*N*-Fe ceramics by the polycondensation of silazane lithium salt with $FeCl_3$.[17] That is the first reported investigation of Fe/Si/C/N ceramics. However, the reaction and isolation of PSZIs are difficult to perform because of the hyperbranched structure and the poor solubility in the synthesis route. In this article, we present a promising alternative polymeric route to obtain PSZIs. The alkyl amide Fe[N(Si-$Me_2Vi)_2]_3$ is easily prepared and isolated, then used in the amine displacement reaction with PVSZ. Consequently, iron is introduced into the polymeric

Correspondence to: Z. Zhang (zhangzj@iccas.ac.cn).
Contract grant sponsor: National Science Foundation of China; contract grant number: 50403027.

precursors successfully. Moreover, vinyl groups in the PVSZ and $Fe[N(SiMe_2Vi)_2]_3$ provide active sites for the heat-induced vinyl crosslinking reactions, resulting in the formation of polymeric precursors that can be pyrolyzed to quaternary Fe/Si/C/N ceramics. Furthermore, it is very facile to obtain precursors with different content of iron by varying the ratio of PVSZ and $Fe[N(SiMe_2Vi)_2]_3$. In addition, the novel magnetic properties of the obtained Fe/Si/C/N ceramics are discussed in detail.

EXPERIMENTAL

Materials

All syntheses were performed under a protective nitrogen atmosphere. Toluene and *n*-hexane were freshly refluxed using Na before use. *n*-Butyllithium (2.5*M* in *n*-hexane) was purchased from Aldrich. $HN(SiMe_2Vi)_2$ and $FeCl_3$ were purchased from Tokyo Kasei Kogyo and used without further purification. PVSZ was from the laboratory stock which was prepared by coammonolysis of Me_2SiCl_2: $ViSiCl_3$ = 1 : 1 in mole ratio.[18]

Synthesis

Synthesis of $Fe[N(SiMe_2Vi)_2]_3$

A modified literature synthesis was used.[19] The solution of $FeCl_3$ (5.41 g, 67 mmol) in 200 mL *n*-hexane was placed in a 500-mL three-necked flask, which was equipped with a dropping funnel and a Teflon-covered magnetic stir. Solid $LiN(SiMe_2Vi)_2$, (19.14 g, 0.1 mol, prepared from *n*-Butyllithium and $HN(SiMe_2Vi)_2$ in *n*-hexane) was slowly added to a suspension of $FeCl_3$ at −20°C over 2 h under magnetic stirring, producing an immediate dark green color. The mixture was allowed to warm to ambient temperature, stirred for 24 h, and then evaporated to dryness *in vacuo*. The oily residue was extracted with dry *n*-pentane (300 mL) and filtered; the filtrate was concentrated to ~ 50 mL and cooled to −20°C to yield dark-green spiculate crystalline $Fe[N(SiMe_2Vi)_2]_3$, which was isolated and dried *in vacuo* (10.24 g). Concentration and cooling of the mother liquor gave a second crop (4.18 g). Total yield of the dark-green, air-sensitive crystals: 14.42 g (71%). Calcd for $C_{24}H_{54}FeN_3Si_6$: C 47.33, H 8.94, N 6.90; found: C 47.04, H 8.84, N 6.82. IR ν: 3376, 3049, 2959, 1594, 1405, 1253, 1180, 1035, 836, 799 cm^{-1}. ^{1}H-NMR (ppm) δ: 0.34(s, 6H, —$SiCH_3$), 4.60–6.40 (br m, 3H, —$SiCH{=}CH_2$). ^{13}C-NMR(ppm) δ: 1.00, 131.26, and 140.82. ^{29}Si-NMR (ppm) δ: −2.34. It should be noted that paramagnetic property of $Fe[N(SiMe_2Vi)_2]_3$ causes obvious broadening of the NMR spectra, which is consistent with the character of the similar compound $Fe[N(SiMe_3)_2]_3$.[19]

Synthesis of PSZIs

Solution of $Fe[N(SiMe_2Vi)_2]_3$ and PVSZ were prepared in anhydrous toluene, and were mixed at room temperature to adjust the amount of $Fe[N(SiMe_2Vi)_2]_3$ in PVSZs to 30, 50, and 70 wt %, identified hereafter as PSZI-30, PSZI-50, and PSZI-70, respectively. With sufficient stirring, the mixtures were heated at 180°C for 2 h. After the evaporation of the solvent and cooling to room temperature, dark-brown fusible PSZI glassy solids were obtained. The yields were 85–95% based on PVSZs.

Crosslinking, pyrolysis of PSZIs

Crosslinking was conducted by heating the PSZIs in a N_2-filled glovebox at 350°C for 5min (heating rate: 10°C min^{-1}) in the absence of any peroxide catalyst. Pyrolysis of the crosslinked samples was performed using an SK-1-10 tube furnace equipped with an Intelligent Universes PID controller and quartz tube. Corundum ceramics boats were used to contain the precursors in the quartz tube. After the samples (3–10 g) were placed into the tube, it was evacuated and purged with N_2 three times before heating. Then the gas flow was controlled at 50 mL min^{-1}. The samples were heated at 1–180°C min^{-1}, then heated at 0.5–350°C min^{-1}, and then heated at 5°C min^{-1} to a final temperature, held at that point for 2 h. Finally, the samples were cooled at 5°C min^{-1} to room temperature.

Characterization

Fourier transfer Infrared (FTIR) spectra were recorded with a PE 2000 IR spectrometer (Perkin–Elmer Cetus Instruments, Norwalk, CT) using KBr-pressed plate. ^{1}H and ^{29}Si NMR spectra were recorded in $CDCl_3$ solution with a Bruker WM 300 spectrometer. ^{13}C NMR spectra were performed in hexane solution. The hydrogen, carbon, and nitrogen content were determined with a Carlo Erba 1106 analyzer. Chemical impact mass spectra were recorded on a Shimadzu instrument (GCMS-QP2010) equipped with a direct inlet. Differential scanning calorimetry (DSC) was recorded on Mettler-Toledo DSC822^e at a heating rate of 10°C min^{-1} and a N_2 purge rate of 50 mL min^{-1}. Thermogravimeter analysis (TGA) was performed using a Perkin-Elmer Pyris 1 TGA, at a heating rate of 10 or 1°C min^{-1} in nitrogen at a rate of 40 mL min^{-1}. X-ray diffraction (XRD) measurements were taken on a powder diffractometer (Rigaku D/M4X 2500) with Cu Kα radiation. Transmission electron microscope (TEM) measurements were conducted on a JEOL 2010 microscope equipped with energy dispersive X-ray analysis (EDX) operated at 200 kV with specimens

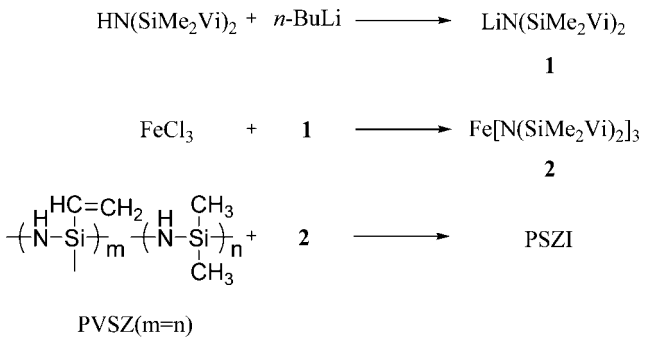

Scheme 1

fabricated by standard preparation techniques (mechanically sectioning the materials, polishing and dimpling the 3 mm discs, which was followed by a final Ar ion beam thinning). The zero-field cooled (ZFC) and field cooled (FC) magnetization measurement was performed using a Quantum Design superconducting quantum interference device (SQUID) magnetometer (MPMS-XL-5), and magnetization versus magnetic field measurements at room temperature were carried out using a vibrating sample magnetometer (LDJ 9600) at room temperature.

RESULTS AND DISCUSSION

Scheme 1 shows the synthetic route for PSZIs investigated in this study. Compared with previous work,[17] the reaction and isolation of $Fe[N(SiMe_2Vi)_2]_3$ are readily realized, and we use the amine displacement reaction along with heat-induced vinyl crosslinking reaction between $Fe[N(SiMe_2Vi)_2]_3$ and PVSZ to synthesize precursors PSZIs. Therefore, the crosslinking of PSZIs is easy to control by reaction temperature and time, which is very important for the manufacture of composite materials.

The IR spectra of PVSZ and PSZI-50 (as an example) are shown in Figure 1. Both of them have absorptions at 3400 cm^{-1} (N—H), 3049 and 1600 cm^{-1} (—Vi), 2950–2900 cm^{-1} (C—H), 1250 cm^{-1} (Si—CH_3), 1170–1180 cm^{-1} (N—H), 930 cm^{-1} (Si—N—Si). Compared with the IR spectrum of PVSZ [Fig. 1(a)], the shoulder signal at near 1035 cm^{-1}, which results from the formation of Si-*N*-Fe bonds,[17] was also detected in that of PSZI-50 [Fig. 1(b)]. However, the substantial presence of unreacted vinyl and NH functions indicates that crosslinking is far from complete.

During the synthesis of PSZIs, simultaneous gas chromatogram studies show the signal of $HN(SiMe_2Vi)_2$ in the evaporated solvent. An ideal reaction can be expressed in Scheme 2 [Eq. (1)]. This ideal amine displacement reaction is on the basis of some similar previous reports.[4,20]

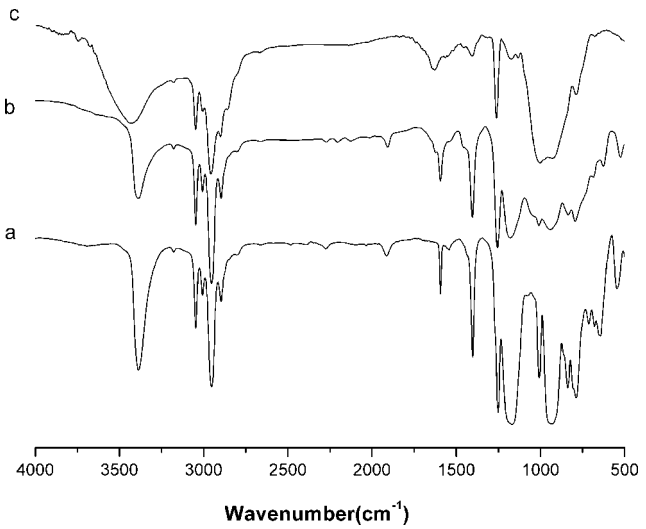

Figure 1 IR spectra of (a) PVSZ, (b) PSZI-50, (c) crosslinked PSZI-50 at 350°C for 5 min.

The crosslinking experiments show that the PSZIs containing a significant portion of vinyl group can be thermally set into a solid products without any catalyst upon heating at 350°C for 5 min (heating rate: 10°C min^{-1}). The most striking feature is the growth of bands around 2950–2900 cm^{-1} (aliphatic C—H stretching), which is correlated with the decrease in the band intensities of vinyl groups (3049 and 1600 cm^{-1}), as revealed by FTIR in Figure 1(c), suggesting the initial crosslinking is mainly because of reaction of vinyl group polymerization in Scheme 2 [Eq. (2)]. Such thermal crosslinking is desirable for ceramic applications, since no contaminating chemicals have to be added to the precursors.

The two reactions in Scheme 2 are also supported by the DSC curves in Figure 2. In the diagram for PSZI-50, one endothermic peak at 150°C and one exothermic peak at 350°C were present, whereas only one exothermic peak at 349°C was observed in the diagram for the pure PVSZ. The peaks near 350°C in both diagrams were contributed to the heat-induced vinyl crosslinking reaction in Scheme 2 [Eq. (2)],

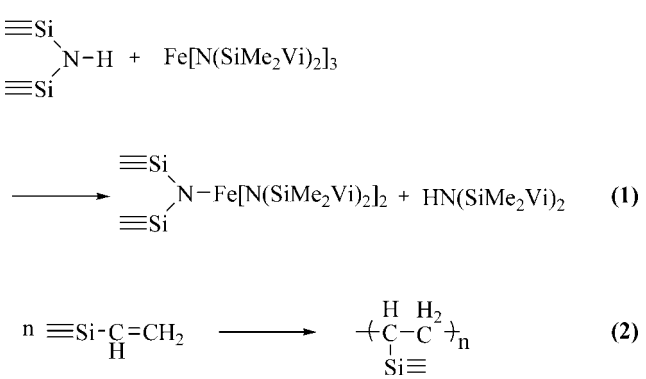

Scheme 2

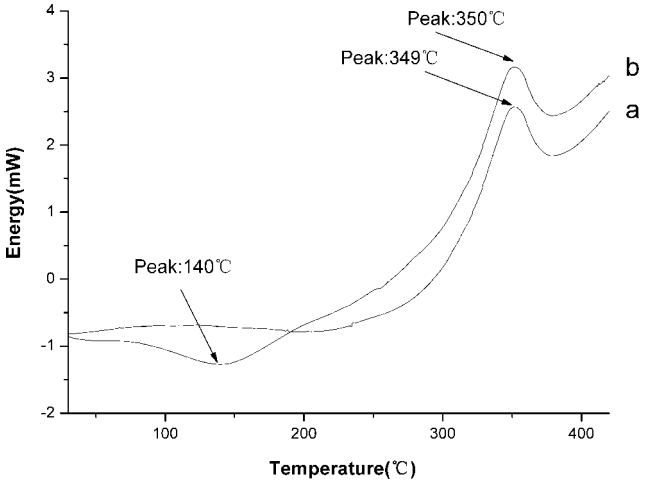

Figure 2 DSC curves of (a) PVSZ, (b) PSZI-50 in N_2 with a heating ratio of 10°C min^{-1}.

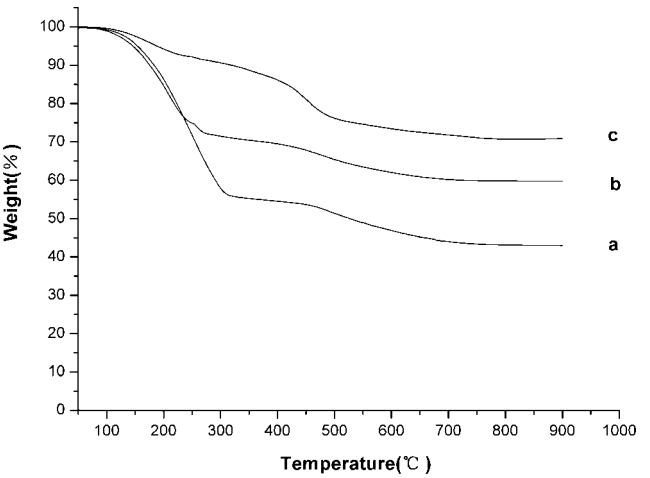

Figure 3 TGA curves of (a) PVSZ (not crosslinked), (b) PSZI-30 (not crosslinked), (c) PSZI-30 (crosslinked) in N_2 with a heating ratio of 10°C min^{-1}.

because vinyl polymerization occurred at much higher temperature (~ 350°C) in polysilazanes that are free of Si—H groups.[21,22] The peak at 150°C in Figure 2(b) was likely to have contributed to the amine displacement reaction in Scheme 2 [Eq. (1)].

To determine the pyrolysis characteristics of the polymeric precursor, TGA of the PVSZ and PSZI-30 (not crosslinked) under N_2 atmosphere have been conducted. Figure 3(a) shows the TGA curve of the neat PVSZ (not crosslinked) up to 900°C at a heating rate of 10°C min^{-1}. The residue at 900°C was black, and the ceramic yield was 43%. Figure 3(b) shows the TGA curve of the precursor PSZI-30 (not crosslinked) up to 900°C at a heating rate of 10°C min^{-1}. The residue at 900°C was shine-black, and the ceramic yield was 60%. Both of the two curves have a three-step mass loss in the following temperature ranges: from room temperature to ~ 200°C, ~ 200–500°C, and from ~ 500°C upwards. And the mass loss for these steps indicates that the decomposition of the organic groups should occur mainly below ~ 500°C, and no further weight loss was detected at temperature above 700°C. Compared with the TGA curve of the neat PVSZ, the precursor PSZI30 has a visible weight maintain about 15% from ~ 200 to 300°C because of crosslinking of the largely introduced reactive —Si—Vi from $Fe[N(SiMe_2Vi)_2]_3$.

Figure 3(c) shows the TGA curve of the crosslinked PSZI-30 up to 900°C at a heating rate of 10°C min^{-1}. The ceramic yield was 71%. Compared with the TGA curve of the precursor PSZI-30 (not crosslinked), the crosslinked PSZI-30 shows a small weight loss during the first weight loss stages. The entire ceramic yield is 71%, which is much higher than 60% observed for the PSZI-30 (not crosslinked). The result suggests that the final yield is dependent of the crosslinking manipulation. As we know, the heating process is also essential for the preparation of ceramics.[23] Based on the weight ratio of the final product to the PSZI-30 precursor, the total ceramic yield after calcinations at 900°C was enhanced from 60 to 72% by reducing the heating rate from 10 to 1°C min^{-1}. This can be attributed to the sufficient crosslinking interactions among the PSZIs at a lower heating rate. Therefore, the heating procedure using the SK-1-10 tube furnace can be optimized to improve the ceramic yield. The loaded PSZIs samples were heated from room temperature to 180°C at 1°C min^{-1}, then to 350°C at 0.5°C min^{-1}, then to their final temperatures at 5°C min^{-1}, which were maintained for 2 h. Finally, the samples were cooled at 5°C min^{-1} to room temperature. Such a pyrolysis process gave yields of the ceramics that were higher than 70% in all samples.

The TEM images of the sample prepared in 500 and 900°C are shown in Figure 4. It indicates nanoparticles embedded in matrix and reveals that the mean size of the nanoparticles prepared at 900°C (~ 20 nm) is obviously larger than that of the nano-

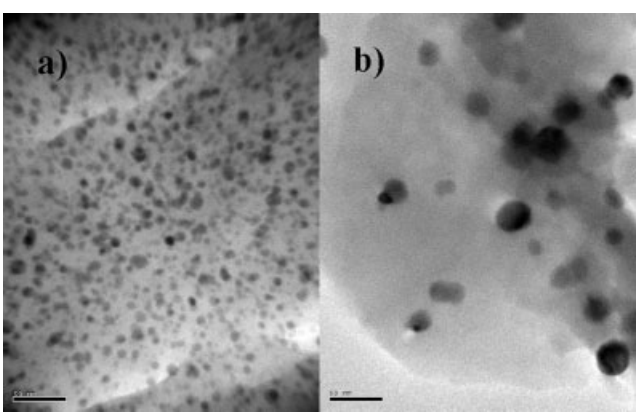

Figure 4 TEM images of the sample prepared at (a) 500°C and (b) 900°C in N_2. The length of the bars is 50 nm.

TABLE I
EDX Analysis of Nanoparticle and Matrix for Features Seen in Figure 4

	Composition (At%)				
	Fe	Si	N	C	O
Nanoparticle	79.60	7.84	0.16	11.69	0.72
Matrix	3.68	27.30	19.07	34.01	15.94

particles prepared at 500°C (~ 5 nm). Table I shows the EDX spectra results of the nanoparticles and matrix in Figure 4. It elucidates: (i) the nanoparticles are identified as Fe-based particles that most contain Fe, and also little Si and C; (ii) the stoichiometry of the matrix is $Fe_{1.0}Si_{7.42}N_{5.18}C_{9.24}O_{4.33.}$ It should be noted a significant content of O is due to the oxidation of the samples in air when they are fabricated and transferred to the microscope.[24]

The X-ray powder diffraction patterns of the pyrolyzed samples in N_2 are shown in Figure 5. The XRD studies of the samples prepared at 500°C showed three low-intensity, broad peaks near $2\theta = 45°$, $2\theta = 65°$, and $2\theta = 82°$[Fig. 5(a)]. These values are very similar to the Fe(110), Fe(200), and Fe(211) reflection of α-Fe (JCPDS file: 06-0696). In Figure 5(b,c), as the temperature increases, the intensities of the peaks due to Fe increase and become sharper. It indicates the growth of grain size of Fe, supported by the Scherrer Eq. (1) given by,

$$d = 0.9\lambda/\beta \cos\theta, \quad (1)$$

where d is the grain size, λ is the wavelength of the radiation used, β is the full width at half-maximum after making the correction due to instrumental broading, and θ is the scattering angle. It is consistent with the TEM images show in Figure 4.

The samples heated below 900°C do not exhibit any significant diffraction peaks of crystallinity from Si/C/N and have a low-intensity, broad peak near $2\theta = 27°$ corresponding to SiO_2 (JCPDS file: 33–1161) in the diffraction pattern. Thus, all these values indicate that α-Fe is the only magnetic crystalline embedded in the amorphous Si/C/*N*-based matrix from 500 to 900°C.

From the TEM images of the sample prepared in 500 and 900°C in Figure 4, it can be elucidated that the growth of α-Fe occurred with the increase of the pyrolysis temperatures. The graphical representation of a nucleation and growth model that illustrates the genesis of the magnetic ceramics has been reported.[25] Upon heating the PSZIs, expansion of the crosslinking precursors occurred; further heating resulted in Fe atom ''release'' from the network because of the facilitating matrix rearrangement and Fe mobility, and the polymer was dismantled as nucleation and growth of the α-Fe particles occurred.

As iron was successfully introduced to the precursor, all the ceramics prepared at ≥500°C under N_2 were attracted to a bar magnet. Therefore, the magnetic properties of these ceramics were investigated with both the vibration sample magnetometer and the SQUID magnetometer. Figure 6 shows magnetization versus magnetic field measurements conducted at room temperature of the samples prepared from PSZI-50 at 500°C in N_2, which indicates that the typical saturation magnetization (M_s), coercivity (H_c), and remanent magnetization (M_r) are 0.50 emu g^{-1}, 51 Oe, and 0.03 emu g^{-1}, respectively. They also show that there is few hysteresis at room temperature and magnetic saturation was gradual, consistent with the behavior of superparamagnetic particles. It was supported by the TEM image of the sample prepared in 500°C in Figure 4(a). It shows that nanoparticles have most sizes less than 5 nm which below the single-domain size for α-Fe.[26] However, the size distribution is quasi-homogeneous with some nanoparticles having diameter above their superparamagnetic limits, which explains the nonzero H_c.

Clear evidence of the superparamagnetic behavior of the sample prepared from PSZI-50 at 500°C in N_2 is given by the ZFC and FC magnetization measurement (applied field = 1000 Oe). In Figure 7, both curves coincide at high temperature and begin to separate as the temperature decrease. It exhibits a maximum in the ZFC at 100 K which is generally ascribed to the average blocking temperature (T_B) of the magnetic moment. Such behavior is characteristic of superparamagnetism.[27] Additionally, the collapse temperatures (the temperature where FC and ZFC curves deviate from each other) are around 130 K. In magnetism, it is generally assumed that T_B depends on the average particle size, while the collapse

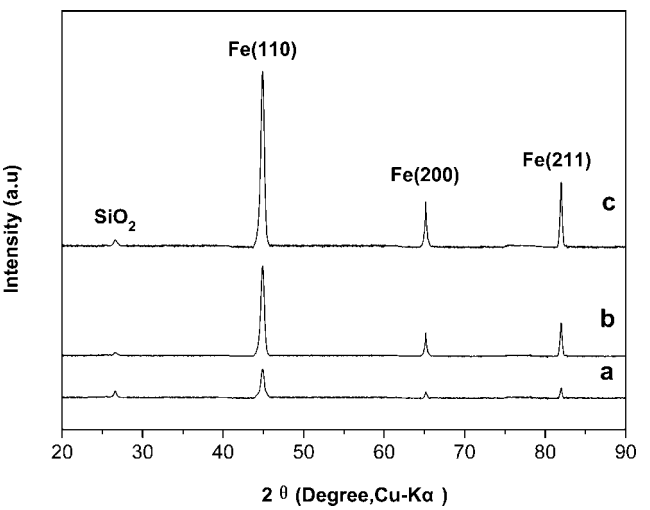

Figure 5 XRD of samples prepared from PSZI-50 at (a) 500°C, (b) 700°C, (c) 900°C in N_2.

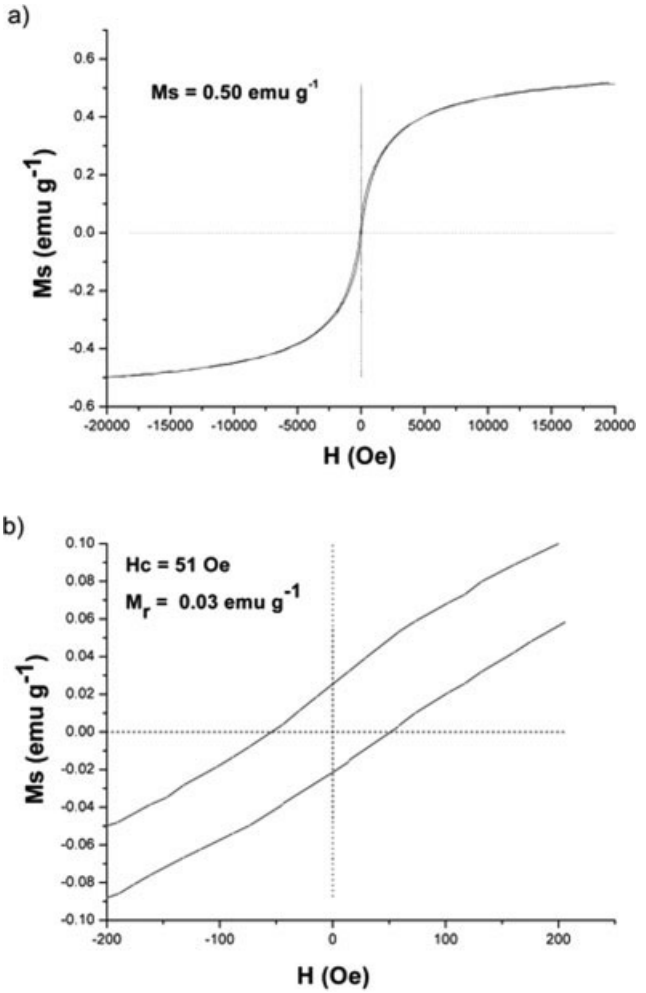

Figure 6 (a) Magnetization versus magnetic field measurements conducted at room temperature for sample prepared from PSZI-50 at 500°C in N_2, (b) the corresponding full range of the hysteresis measured between −200 and 200 Oe.

temperature corresponds to the largest particles.[28] The difference between both temperatures is confirmed by the quasi-homogeneous size distribution of the α-Fe particles shows in Figure 4(a).

Figure 8 shows magnetization versus magnetic field measurements conducted at room temperature of the samples prepared from PSZI-70 at different temperatures in N_2. The saturation magnetization(M_s) of the samples increases from 0.75 to 17.25 emu g^{-1} gradually when the pyrolysis temperature varies from 500 to 900°C. Lower values of the samples prepared from PSZI-50 were observed in Table II as expected with the introduction of less iron. Therefore, by varying the pyrolysis temperature and the content of the introduced iron, the magnetic properties of the resulting ceramics could be tuned. This flexibility may be advantageous for particular magnetic materials applications.

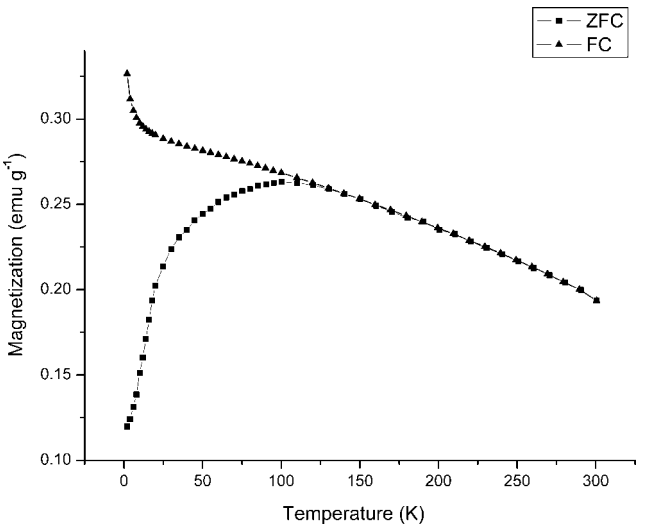

Figure 7 Zero-field cooled (ZFC) and field cooled (FC) magnetization curves of the sample prepared from PSZI-50 at 500°C in N_2. The sample was cooled and measured in an applied field of 1000 Oe.

CONCLUSIONS

In summary, we have demonstrated a facile synthetic route to the formation of PSZI, and they can be converted to Fe/Si/C/N ceramics with tunable magnetic properties by controlling the content of introduced iron and the pyrolysis temperature. Results show the small α-Fe particles embed in ceramics prepared from 500 to 900°C and the sample prepared at 500°C exhibit superparamagnetic behavior. These magnetic ceramics may be a candidate for applications in some magnetic field, such as magnetic recording and magnetic shielding applications in the future.

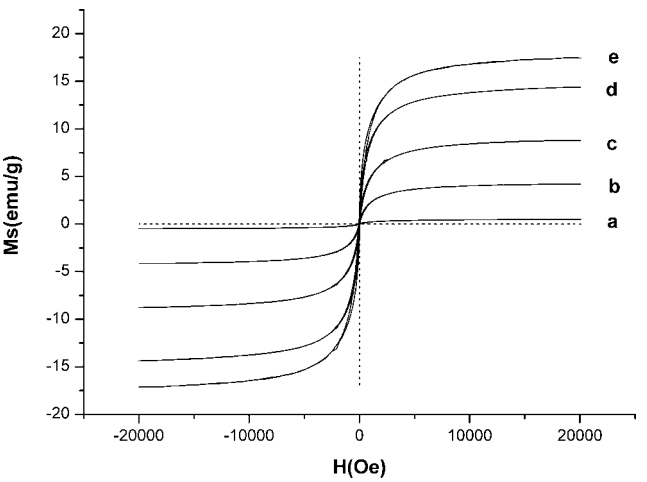

Figure 8 Magnetization versus magnetic field measurements conducted at room temperature for samples prepared from PSZI-70 at (a) 500°C, (b) 600°C, (c) 700°C, (d) 800°C, and (e) 900°C in N_2.

TABLE II
Magnetic Parameters (M_s) at Room Temperature Variation With the Pyrolysis Temperature and the Content of the Introduced Iron

	M_s (emu g^{-1})				
Samples	500°C	600°C	700°C	800°C	900°C
PSZI-50	0.50	3.21	5.52	6.24	12.88
PSZI-70	0.75	4.17	8.78	14.36	17.25

The authors thank Dr. Yi Qiao (State Key Laboratory for Advanced Metals and Materials, University of Science and Technology Beijing) for her helpful contribution on vibrating sample magnetometer analyses and useful discussions.

References

1. Yajima, S.; Hayashi, J.; Omori, M. Chem Lett 1975, 931.
2. Yajima, S.; Hayashi, J.; Omori, M.; Okamura, K. Nature 1976, 261, 683.
3. Loffelholz, J.; Jansen, M. Adv Mater 1995, 7, 289.
4. Hapke, J.; Ziegler, G. Adv Mater 1995, 7, 380.
5. Lang, H.; Seyferth, D. Appl Organomet Chem 1990, 4, 599.
6. Thorne, K.; Liimatta, E.; Mackenzie, J. D. J Mater Res 1991, 6, 2199.
7. Janakiraman, N.; Hoche, T.; Grins, J.; Esmaeilzadeh, S. J Mater Chem 2006, 16, 3844.
8. Ripka, P.; Vertesy, G. J Magn Magn Mater 2000, 215/216, 795.
9. Kim, S.-S.; Kim, S.-T.; Ahn, J.-M.; Kim, K.-H. J Magn Magn Mater 2004, 271, 39.
10. Bruce, I. J.; Taylor, J.; Todd, M.; Davies, M. J.; Borioni, E.; Sangregorio, C.; Sen, T. J Magn Magn Mater 2004, 284, 145.
11. Kim, H.-J.; Ahn, J.-E.; Haam, S.; Shul, Y.-G.; Song, S.-Y.; Tatsumi, T. J Mater Chem 2006, 16, 1617.
12. Corriu, R. J. P.; Devylder, N.; Guerin, C.; Henner, B.; Jean, A. J Organomet Chem 1996, 509, 249.
13. MacLachlan, M. J.; Ginzburg, M.; Coombs, N.; Coyle, T. W.; Raju, N. P.; Greedan, J. E.; Ozin, G. A.; Manners, I. Science 2000, 287, 1460.
14. MacLachlan, M. J.; Ginzburg, M.; Coombs, N.; Raju, N. P.; Greedan, J. E.; Ozin, G. A.; Manners, I. J Am Chem Soc 2000, 122, 3878.
15. Manners, I. Science 2001, 294, 1664.
16. Clendenning, S. B.; Han, S.; Coombs, N.; Paquet, C.; Rayat, M. S.; Grozea, D.; Brodersen, P. M.; Sodhi, R. N. S.; Yip, C. M.; Lu, Z. H.; Manners, I. Adv Mater 2004, 16, 291.
17. Li, Y. M.; Zheng, Z. M.; Reng, C. Y.; Zhang, Z. J.; Gao, W.; Yang, S. Y.; Xie, Z. M. Appl Organomet Chem 2003, 17, 120.
18. Zheng, Z. M.; Li, Y. M.; Luo, Y. M.; Su, S. X.; Zhang, Z. J.; Yang, S. Y.; Gao, W.; Xie, Z. M. J Appl Polym Sci 2004, 92, 2733.
19. Duncan, J. S.; Nazif, T. M.; Verma, A. K.; Lee, S. C. Inorg Chem 2003, 42, 1211.
20. Seyferth, D.; Mignani, G. J Mater Sci Lett 1988, 7, 487.
21. Bill, J.; Seitz, J.; Thurn, G.; Durr, J.; Canel, J.; Janos, B. Z.; Jalowiecki, A.; Sauter, D.; Schempp, S.; Lamparter, H. P.; Mayer, J.; Aldinger, F. Phys Status Solidi A Appl Res 1998, 166, 269.
22. Li, Y. L.; Kroke, E.; Riedel, R.; Fasel, C.; Gervais, C.; Babonneau, F. Appl Organomet Chem 2001, 15, 820.
23. Bahloul, D.; Pereira, M.; Goursat, P.; Choong, N. S.; Yive, K.; Corriu, R. J. P. J Am Ceram Soc 1993, 76, 1156.
24. Diaz, L.; Santos, M.; Ballesteros, C.; Marysko, M.; Pola, J. J Mater Chem 2005, 15, 4311.
25. Ginzburg, M.; MacLachlan, M. J.; Yang, S. M.; Coombs, N.; Coyle, T. W.; Raju, N. P.; Greedan, J. E.; Herber, R. H.; Ozin, G. A.; Manners, I. J Am Chem Soc 2002, 124, 2625.
26. LesliePelecky, D. L.; Rieke, R. D. Chem Mater 1996, 8, 1770.
27. Morup, S.; Bodker, F.; Hendriksen, P. V.; Linderoth, S. Phys Rev B 1995, 52, 287.
28. Salgueiriño-Maceira, V.; Correa-Duarte, M. A.; Spasova, M.; Liz-Marzán, L. M.; Farle, M. Adv Funct Mater 2006, 16, 509.